European Journal of Medicinal Chemistry 165 (2019) 80–92

Contents lists available at ScienceDirect

European Journal of Medicinal Chemistry

journal homepage: http://www.elsevier.com/locate/ejmech

Research paper

Rad51/BRCA2 disruptors inhibit homologous recombination and synergize with olaparib in pancreatic cancer cells

Marinella Roberti [a], Fabrizio Schipani [b], Greta Bagnolini [a, b], Domenico Milano [b], Elisa Giacomini [b], Federico Falchi [b, 1], Andrea Balboni [b, c], Marcella Manerba [c], Fulvia Farabegoli [a], Francesca De Franco [d], Janet Robertson [d], Saverio Minucci [e, f], Isabella Pallavicini [e], Giuseppina Di Stefano [c], Stefania Girotto [b], Roberto Pellicciari [d], Andrea Cavalli [a, b, *]

[a] Department of Pharmacy and Biotechnology, University of Bologna, Via Belmeloro 6, 40126, Bologna, Italy
[b] Computational & Chemical Biology, Istituto Italiano di Tecnologia, via Morego 30, 16163, Genova, Italy
[c] Department of Experimental, Diagnostic and Specialty Medicine, University of Bologna, Via S. Giacomo 14, 40126, Bologna, Italy
[d] TES Pharma S.r.l., Via Palmiro Togliatti 22bis, I-06073, Loc. Terrioli, Corciano, Perugia, Italy
[e] Department of Experimental Oncology at the European Institute of Oncology, IFOM-IEO Campus, Via Adamello 16, 20100, Milan, Italy
[f] Department of Biosciences, University of Milan, Via Celoria 26, 20100, Milan, Italy

ARTICLE INFO

Article history:
Received 19 October 2018
Received in revised form
3 January 2019
Accepted 4 January 2019
Available online 10 January 2019

Keywords:
Synthetic lethality
Homologous recombination
Protein-protein small molecule inhibitors
Anticancer drugs
PARP inhibitors

ABSTRACT

Olaparib is a PARP inhibitor (PARPi). For patients bearing BRCA1 or BRCA2 mutations, olaparib is approved to treat ovarian cancer and in clinical trials to treat breast and pancreatic cancers. In BRCA2-defective patients, PARPi inhibits DNA single-strand break repair, while BRCA2 mutations hamper double-strand break repair. Recently, we identified a series of triazole derivatives that mimic BRCA2 mutations by disrupting the Rad51-BRCA2 interaction and thus double-strand break repair. Here, we have computationally designed, synthesized, and tested over 40 novel derivatives. Additionally, we designed and conducted novel biological assays to characterize how they disrupt the Rad51-BRCA2 interaction and inhibit double-strand break repair. These compounds synergized with olaparib to target pancreatic cancer cells with functional BRCA2. This supports the idea that small organic molecules can mimic genetic mutations to improve the profile of anticancer drugs for precision medicine. Moreover, this paradigm could be exploited in other genetic pathways to discover innovative anticancer targets and drug candidates.

1. Introduction

In the past two decades, cancer research has focused on discovering tumor-specific signaling and metabolic pathways that might be exploited for pathway-targeted anticancer therapies [1,2]. To date, regulators have approved several small molecules and monoclonal antibodies, which directly inhibit genes and proteins that are critical in oncogenic signal networks. These have increased survival in patients with previously intractable cancers [3–8]. However, the first generation of targeted therapies have some limitations, including the development of resistance and on- and off-target toxicities [9,10]. Therefore, researchers are increasingly turning to precision medicine, using genetic changes in a patient's tumor to determine their treatment.

Synthetic lethality is a new concept with great potential for discovering new anticancer molecules within the framework of precision medicine. Synthetic lethality arose from genetic studies in model organisms. Two genes are synthetically lethal if the perturbation of either gene alone is compatible with cell viability, but simultaneous perturbation of both genes leads to cell death. In principle, it is possible to use a small molecule to target the synthetically lethal partner of an altered gene in cancer cells but not in normal cells. This should selectively kill cancer cells while sparing normal cells [11–14].

* Corresponding author. Department of Pharmacy and Biotechnology, University of Bologna, Via Belmeloro 6, 40126, Bologna, Italy.
E-mail address: andrea.cavalli@iit.it (A. Cavalli).
[1] Present address: Molecular Horizon srl, Via Montelino 30, 06084 Bettona (PG), Italy.

https://doi.org/10.1016/j.ejmech.2019.01.008
0223-5234/

One example of synthetic lethality is the use of poly [ADP-ribose] polimerase (PARP) inhibitors in oncology patients with BRCA1/2 mutations (Fig. 1A). BRCA2 is important for repairing DNA double-strands breaks (DSBs) by homologous recombination (HR), whereas PARP is important for repairing single-strand breaks. Synthetic lethality arises from the simultaneous impairment of the repair mechanisms for single-strand and double-strand breaks. Developed by AstraZeneca, olaparib (Lynparza™, Fig. 1A) was the first PARP inhibitor (PARPi) approved to treat advanced ovarian cancer associated with defective BRCA genes [15]. Several clinical trials are now studying olaparib to treat breast and pancreatic tumors associated with germline BRCA mutations [16].

One of BRCA2's key mechanisms is to recruit Rad51, an evolutionarily conserved recombinase that uses HR to repair double-strand breaks [17]. In parallel, Rad51 overexpression has been reported in a wide variety of cancers (e.g. breast, pancreatic), where enhanced HR activity has been observed [18]. Rad51 and BRCA2 interact through eight well-conserved motifs, namely the BRC repeats [19,20]. The X-ray crystallographic structure of BRC4 (the fourth BRC repeat) is available in complex with the catalytic domain of Rad51 [21]. This makes the Rad51-BRCA2 interaction suitable for the structure-based design of small molecule disruptors. Indeed Lee et al. recently identified a small molecule inhibitor of Rad51-BRCA2 for potential cancer treatment [22,23].

In this context, we recently proposed a new anticancer drug discovery concept, which combines Rad51-BRCA2 disruptors with olaparib to mimic the synthetic lethality described above (Fig. 1B) [24]. Our working hypothesis was that, by disrupting the Rad51-BRCA2 interaction, we could make cancer cells more sensitive to PARPi, DNA-damaging agents, and radiotherapy. In particular, we reasoned that, by administering Rad51-BRCA2 disruptors to individuals without BRCA mutations, it would be possible to mimic the enhanced sensitivity to PARPi observed in BRCA2-defective oncology patients. Due to their increased genetic instability, cancer cells experience DNA damage more frequently than healthy cells. They should therefore be preferentially affected by the inhibition of DNA repair produced by the synergy of olaparib and the Rad51-BRCA2 disruptors.

We first carried out a virtual ligand screening campaign using commercial databases (Asinex and Life Chemical databases; overall more than 1.5 millions of compounds), which allowed us to identify potential triazole-based hit compounds. Subsequent ELISA biochemical assay showed that **1** (Fig. 2) was able to disrupt the Rad51-BRCA2 interaction. Preliminary modification of the linker connecting the triazole and the phenyl ring led to the propyl phenyl derivative **2**, which was studied at the cellular level. In line with our hypothesis, **2** increased the sensitivity to olaparib in cancer cells BxPC-3 with fully functional BRCA2 [24]. This synergistic effect was not observed in Capan-1, pancreas adenocarcinoma cells that lack functional BRCA2.

To discover more effective compounds, we here design and synthesize a library of new triazole analogues (**3**–**42,** Tables 1–2). In particular, we attempt to depict general structure-activity relationships (SAR) of **3**–**42** in inhibiting the Rad51-BRCA2 interaction. Additionally, we also report on novel biological investigations to further elucidate the mechanistic aspects of the synergistic activity of Rad51-BRCA2 disruptors and PARPi.

2. Results and discussion

2.1. Design approach

Targeting protein-protein interactions (PPI) is an attractive strategy for designing innovative drugs for highly complex diseases, such as cancer [25]. However, it is rather difficult to identify and optimize PPI disruptors. This is because proteins usually interact with other proteins via shallow surface sites. This makes it difficult to optimize ligands using classic structure-based approaches. To improve binding at surface sites, many weak interactions must be optimized. In-depth studies of the target structure may identify surface pockets as hot spots to be targeted. We identified a potentially suitable pocket, often referred to as the “FxxA pocket”. This pocket is one of the two Rad51 regions where BRC4 (i.e. the fourth BRC repeat responsible for binding of BRCA2 to Rad51) [24] binds its counterpart. This structural analysis prompted us to run a virtual screening campaign based on high-throughput docking at the FxxA pocket in order to identify Rad51-BRCA2 disruptors. With this strategy, we discovered a series of triazole-based compounds. **1** and **2** were selected as initial hit candidates [24]. Notably, triazoles bear a peculiar structure that makes them particularly suited to

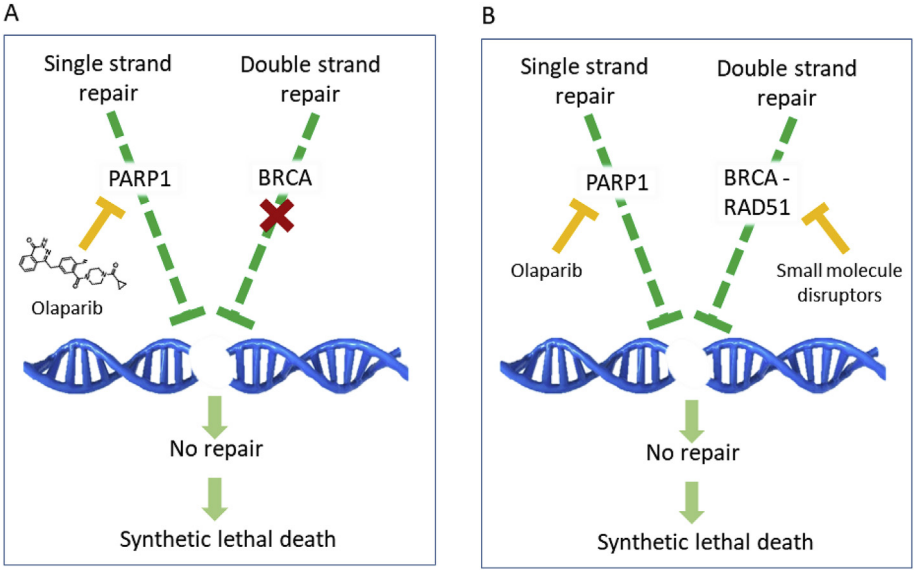

Fig. 1. a) Mechanism of synthetic lethal death induced by the PARP inhibitor olaparib in BRCA-defective cancer cells. b) Mechanism of synthetic lethal death triggered by a combination of olaparib and BRCA2-RAD51 disruptors. In this case, synthetic lethality is fully triggered by small organic molecules.

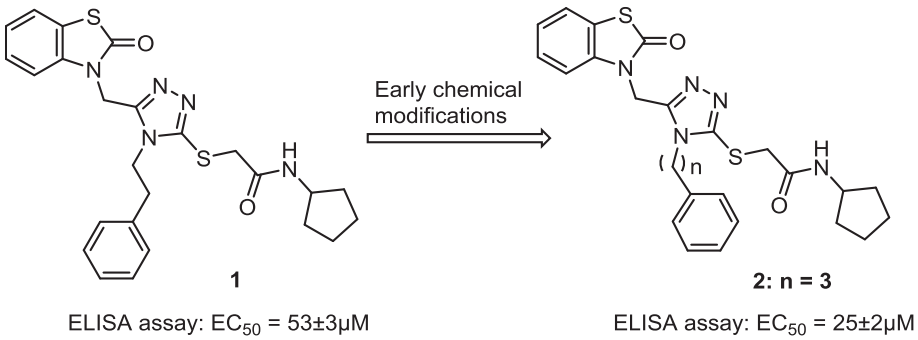

Fig. 2. Structure of the previously identified **1** and **2**.

disrupting protein-protein interactions [26–28]. The binding mode of **1** to Rad51 (Fig. 3a), as obtained by docking simulations, shows noticeable similarities to the crystallographic structure of Rad51 in complex with BRC4. Specifically, the docking model suggests that (i) the phenyl ring of the ethyl phenyl group of **1** binds (similarly to the Phe1524 of BRC4) into the hydrophobic pocket outlined by the side chains of Met158, Ile160, Ala190, Leu203, Ala207, and Met210 of Rad51; (ii) the carbonyl group of the benzothiazolone moiety forms hydrogen bonds with the sidechains of Rad51, His199, and Gln206, similarly to the backbone carbonyl of Leu1522 of BRC4. Likewise, (iii) the acetamide carbonyl of **1** binds the backbone Tyr191 of Rad51, similarly to His1525 of BRC4.

To improve the protein-protein inhibitory activity of **1**, we conducted a chemical modification campaign around the triazole moiety. Fig. 3b provides an overview of the structural variants introduced on the triazole scaffold.

First, several different acetamide chains were introduced in position 3 (blue region, Fig. 3b) bearing different heterocycles, saturated or unsaturated rings, leaving the carbonyl group unchanged (**3**–**10,** Table 1). Additionally, to investigate its role, the acetamide function was removed (**11,** Table 1). Regarding position 4 (red region, Fig. 3b), the first set of structural changes involved introducing different substituents (namely methyl, hydroxyl, and fluorine) on the phenyl ring, while retaining the two carbons ethyl chain (**12**–**18,** Table 1). In position 5 (green region, Fig. 3b), the methylene benzothiazolone moiety was removed or replaced with other aromatic rings to probe its role (**19**–**22,** Table 1). Moreover, the methylene benzothiazolone moiety was modified by introducing different substituents on the aromatic ring, including hydroxy and methoxy groups and a fluorine atom (**23**–**25,** Table 1).

Based on the promising biological activities of the 4-N-propyl phenyl triazole derivative **2**, a second set of compounds was envisaged (**26**–**42**). Similarly to compound **1**, modifications were made to the moieties in position 3 (**26**–**32**) and 5 (**33**–**39**) of the triazole ring, leaving the linear propyl chain in position 4 unchanged. Moreover, the phenyl fragment of the propyl phenyl region in position 4 was substituted by 2, 3 and 4 pyridine moieties (**40**–**42**) (Fig. 3b).

2.2. Chemistry

Scheme 1 illustrates the common synthetic strategy for achieving most of the desired compounds (**3**–**21, 23, 25**–**36, 38**–**42**). Hydrazides **43a-n** and the appropriate isothiocyanates **44a-l** underwent cyclocondensation in the presence of triethylamine to give 1,2,4-triazole-3-thiol intermediates **45**–**69**. S-alkylation of **45**–**55, 57**–**63,** and **65**–**69** with 2-chloro-acetamides **70a-m** led to final compounds **3**–**21, 23, 25**–**36,** and **38**–**42**. The 5-methoxybenzothiazolone derivative **23** was in turn treated with BBr_3 to obtain the corresponding hydroxy analog **24** (see Supporting Information Scheme S1). Compounds **22** and **37** were obtained from the Boc-protected 1,2,4-triazole-3-thiol intermediates **56** and **64**, which were alkylated with 2-chloro-N-cyclopentylacetamide **70l** to afford the corresponding derivatives **71**–**72**. In turn, **71**–**72** were Boc-deprotected to afford the final **22**, **37** respectively (see Supporting Information Scheme S2). The hydrazides **43a-j**, not commercially available, were obtained by reaction of hydrate NH_2NH_2 with the corresponding methyl, ethyl, or benzyl ester **73a-j** (Scheme 2). The esters **73a-j** were obtained by nucleophilic substitution reaction between the appropriate amine **74a-i** and benzyl, ethyl, or methyl bromoacetate **75**, **76**, and **77** respectively. In addition to the desired **73i,** the reaction between the substituted pyridinone **74i** and methyl bromoacetate **77** unexpectedly provided the substituted pyridine methyl 2-oxiacetate **73j** (Scheme 2, entry 9). **73i** and **73j** were separated and treated with hydrate NH_2NH_2 to afford the corresponding hydrazides **43i** and **43j**. The hydrazide **43k**, which is not commercially available, was prepared from the Boc-aminomethyl ester **78** according to general procedure. **78** was obtained by the esterification of aminomethyl benzoic acid **79**, which was refluxed with ethanol in the presence of HCl to achieve the amino ester **80**. In turn, **80** was protected with *tert*-butyloxycarbonyl (Boc) group to afford **78** (see Supporting Information Scheme S3). The isothiocyanates **44a-j** were not commercially available and were obtained by reaction of the appropriate amine **81a-j** with 1,1-thiocarbonyldimidazole **82** (Scheme 3). The chloroacetamides **70a-h**, not commercially available, were obtained through nucleophilic substitution reaction between the appropriate amine **83a-h** and chloroacetyl chloride **84** (Scheme 4).

2.3. Biological evaluation

Our working hypothesis is that small molecule disruptors of Rad51-BRCA2 could synergize with PARPi to treat ovarian, breast, and pancreatic cancers. Here, we focused on pancreatic cancer because it is an unmet oncological need. To investigate the mechanism of action of the new triazole derivatives, different biological assays were performed. First, the ability of compounds **3**–**42** to inhibit Rad51-BRCA2 interaction was investigated with a competitive biochemical ELISA assay against parent compounds **1** and **2** (Tables 1–2). This assay is effective in evaluating the ability of new molecules to compete with BRC4 to bind to Rad51 [24].

For the 4-N-ethyl phenyl triazole series (**3**–**25**, Table 1), all compounds were inactive, with the exception of 3-thio-N-phenylacetamide **3** and 4-N(2-methyphenethyl) **16** derivatives, which were active in the high micromolar range. These data indicate that no improvement in Rad51-BRCA2 inhibitory activity was achieved with this new series of compounds relative to the parent

Table 1
Structures and EC_{50} of compounds **3**–**25** on ELISA Assay.

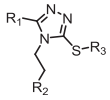

Cp	R_1	R_2	R_3	EC_{50} (μM)[a]
3				95 ± 5
4				n.a.[b]
5				n.a.[b]
6			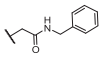	n.a.[b]
7				n.a.[b]
8				n.a.[b]
9			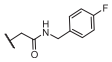	n.a.[b]
10				n.a.[b]
11				n.a.[b]
12				n.a.[b]
13				n.a.[b]
14				n.a.[b]
15				n.a.[b]
16				100 ± 10
17				n.a.[b]
18				n.a.[b]
19				n.a.[b]
20				n.a.[b]
21				n.a.[b]
22				n.a.[b]
23				n.a.[b]
24				n.a.[b]
25				n.a.[b]

[a] All points were tested in triplicate with error bars indicating the standard deviation.
[b] Not active.

compound, **1** (EC_{50} = 53 ± 3 μM).

For the series of the 4-N-propyl phenyl triazoles (**26**–**42,** Table 2), 3-thio-N-cyclohexylacetamide **26** showed fairly good potency with an EC_{50} of 8 ± 2 μM, three-fold higher than the parent 3-thio-N-cyclopentylacetamide **2** (EC_{50} = 25 ± 2 μM). The binding mode of these two compounds, obtained by docking simulations, is reported in the Supporting Information (Fig. S1). **27** and **28** were active in the micromolar range (EC_{50} of 24 ± 5 μM and 42 ± 2, respectively), both very similar to the initial hit. Therefore, activity is marginally affected by replacing the cyclopentyl ring in the 3-thio-N-cyclopentylacetamide chain with different cycloalkyl rings

Table 2
Structures and EC_{50} of compounds **26**–**42** on ELISA Assay.

Cp	R_1	R_2	R_3	EC_{50}(μM)[a]
26				8 ± 2
27				24 ± 5
28				42 ± 3
29				n.a.[b]
30				n.a.[b]
31				n.a.[b]
32				n.a.[b]
33				n.a.[b]
34				90 ± 5
35				n.a.[b]
36				n.a.[b]
37				n.a.[b]
38				n.a.[b]
39				33 ± 7
40				n.a.[b]
41				n.a.[b]
42				n.a.[b]

[a] All points were tested in triplicate with error bars indicating the standard deviation.
[b] Not active.

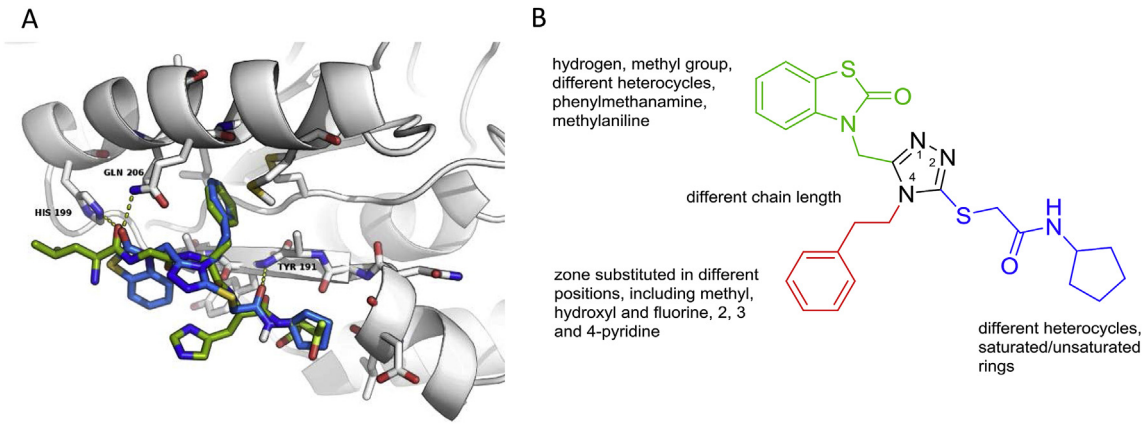

Fig. 3. a) Compound **1** docked into the FxxA domain of Rad51. The small molecule recapitulates major interactions the peptide BRC4 establishes with the biological target. b) Overview of the optimization strategy of **1** for SAR exploration. **2** was investigated in a similar way to **1**, leaving the linear propyl chain in position 4 unchanged.

such as cyclohexyl (**26**), cyclopropyl (**27**), and cyclobutyl (**28**). Replacing the methylene benzothiazolone moiety yielded compounds that had reduced inhibitory activity (**34**, $EC_{50} = 90 \pm 5$ μM and **39** $EC_{50} = 33 \pm 7$ μM) or were fully inactive (**33**, **35**–**38**). For compounds **40**, **41**, and **42**, the phenyl of the propyl phenyl group was replaced by a 2, 3, or 4-pyridine ring, respectively. These compounds were inactive. As expected, PPI disruptors are very difficult to obtain and optimize. Moreover, it is challenging to properly depict meaningful SAR. Indeed, slight modifications of active compounds led on the one hand to molecules that were either fully inactive or with greatly reduced inhibitory activity, while on the other hand to molecules with improved potency. However, further modifying compounds in that direction did not necessarily provide reasonable SAR. Protein-protein disruptors usually bind the target at shallow surface sites, and potency against the target is usually dictated by many weak interactions. Therefore, it is challenging to identify the optimal pool of substituents that a small molecule should bear in order to recapitulate the protein-protein interactions. Despite this, we slightly improved the biological profile of the initial compound (**2**), as per the biological investigations reported below.

Compounds **26**, **27**, **28,** and **39** were submitted to cell-based studies. **28** and **39** were discarded because of poor solubility. **26** and **27** were characterized in human pancreatic carcinoma, using BxPC3 cells. These cells were chosen for their clinical relevance and for the possibility of using Capan-1 cells [29], which lack functional BRCA2 protein and could therefore serve as negative control. Additionally, BxPC3 and Capan-1 match well in terms of tumor type and differentiation state [29].

The Rad51-BRCA2 interaction is crucial in recruiting the recombinase Rad51 to cell nuclei, where it uses homologous recombination (HR) to repair double-strand breaks. We therefore studied HR inhibition in BxPC3 and Capan-1 cells. The assay is based on cell transfection with two plasmids bearing the LacZ sequence, each with a different mutation. In transfected cells, the recombination machinery restores the corrected LacZ sequence, which can be detected by PCR. Using two different primer sets, both the plasmid couple and the recombination product can be measured, allowing an estimation of HR efficiency. This assay was applied to cells treated (16 h) with **2** and with the two new triazole structures (**26** and **27**) as shown in Fig. 4A.

Unexpectedly, **2** increased the HR rate in treated cells, presumably by causing direct DNA damage via off-target activities. Conversely, **26** and **27** reduced HR in treated BxPC3 cells suggesting their potential ability to disrupt Rad51-BRCA2 interaction in living cells too. Of the two molecules, **26** had the strongest effect, with a statistically significant 40% inhibition at 20 μM. **27** showed a less marked effect, with a 24% inhibition at 40 μM. The limited solubility of **27** further hindered a dose escalation with this compound. Neither **26** nor **27** inhibited HR in Capan-1 cells (see Supporting Information, Figure S2), which lack functional BRCA2. This strongly supports their mechanism of action as being the disruption of the Rad51-BRCA2 interaction. These data also suggested that **26** and **27** were potentially capable of synergizing with olaparib in pancreatic cancer cells with functional BRCA2, where olaparib usually is inactive. The two compounds were therefore tested in BxPC3 and Capan-1 cell viability experiments in combination with olaparib. Fig. 4B reports the results after 72 h exposure to treatments. **27** did not affect olaparib efficacy. However, **26** significantly increased olaparib efficacy in BxPC3 cells, without affecting its efficacy in the BRCA2-defective cells (Capan-1). These results further confirm, in a dose-dependent manner, that HR inhibition might explain the synergistic effect of combining Rad51-BRCA2 disruptors with PARPi in cell lines with fully functional BRCA2, where PARPi are usually inactive. Further experiments were conducted on **26** to confirm the synergy with olaparib.

By adopting a longer exposure time to treatments (144 h), we assessed how the **26**/olaparib combination affected cell viability and cell death (Fig. 5A). Cell death was evaluated using the CellTox Green Dye (Promega) probe, which emits a fluorescence signal only in the presence of cells with impaired membrane integrity. Again, we observed a statistically significant increase in olaparib's power in reducing cell viability. The data of the cell viability experiment plotted in Fig. 5A were also used to evaluate the combination index (CI) between olaparib and **26**. Following the procedure described previously [24], a CI value of 0.76 ± 0.03 was obtained, which suggests a potential synergistic effect between the compounds.

However, the enhanced olaparib potency did not produce evidence of increased cell death. An immunoblotting evaluation of apoptosis markers confirmed this result (See Supporting Information, Fig. S3). Using the same exposure time to treatments, an immunoblotting evaluation of DNA damage was also performed by measuring the phosphorylation of H2AX (γ-H2AX), a sensitive and universal indicator of DNA double-strand break formation [30]. Results are reported in Fig. 5B. The densitometric evaluation of γ-H2AX bands, normalized on actin levels, have been plotted in the bar graph. It shows that, in cells treated with the combination of olaparib with **26**, the DNA damage signal was >70% higher than that observed in control and in olaparib-treated cells. This experiment also showed that, when given as a single treatment, **26** did not

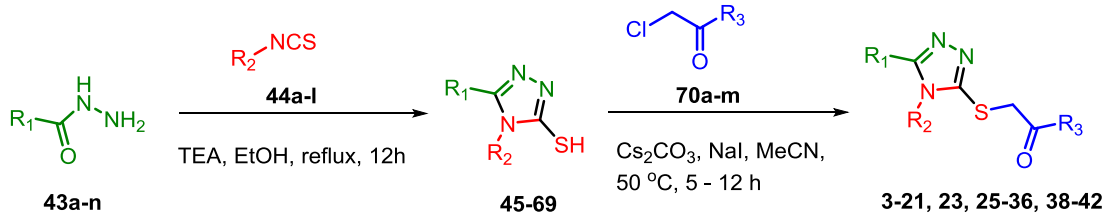

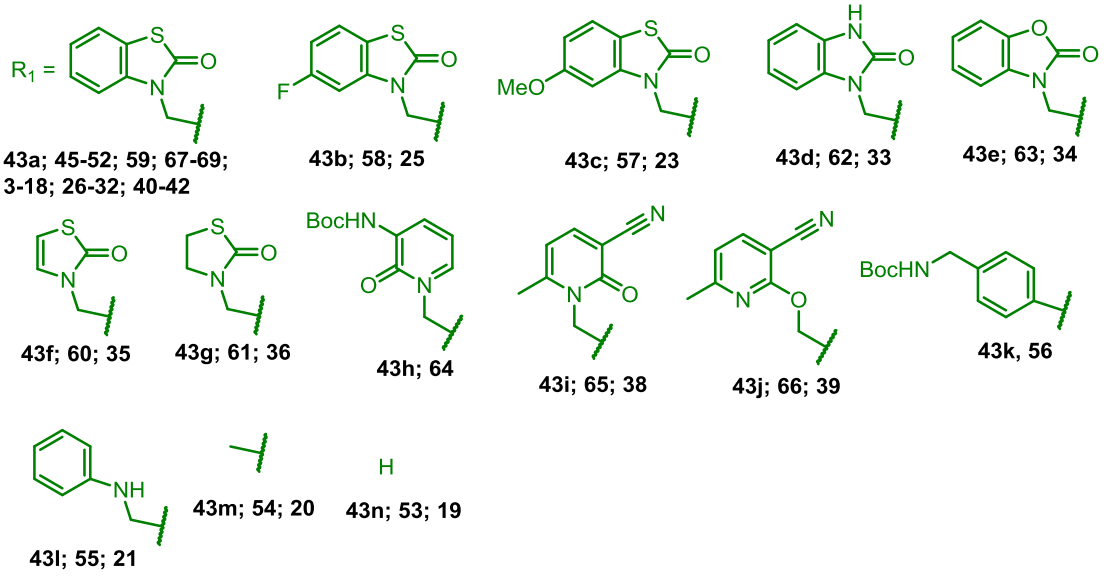

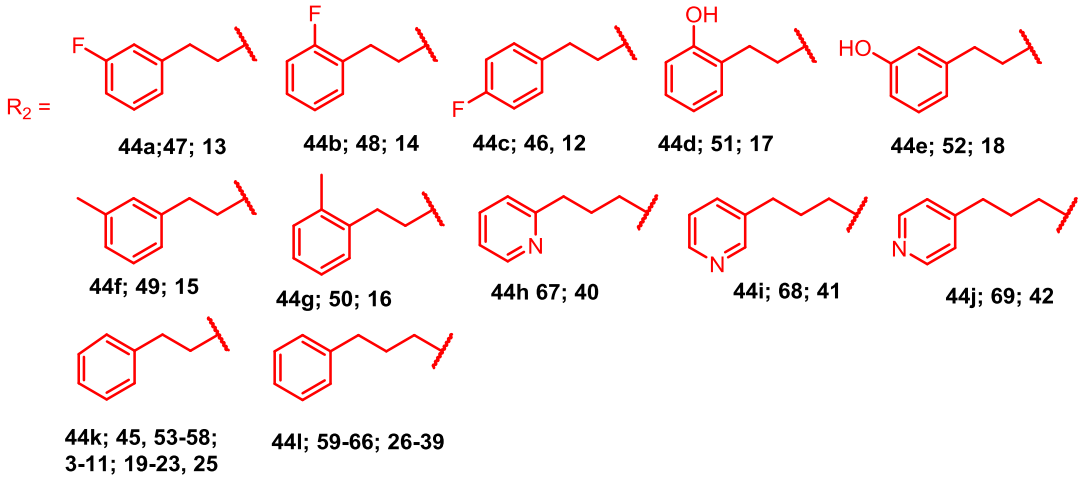

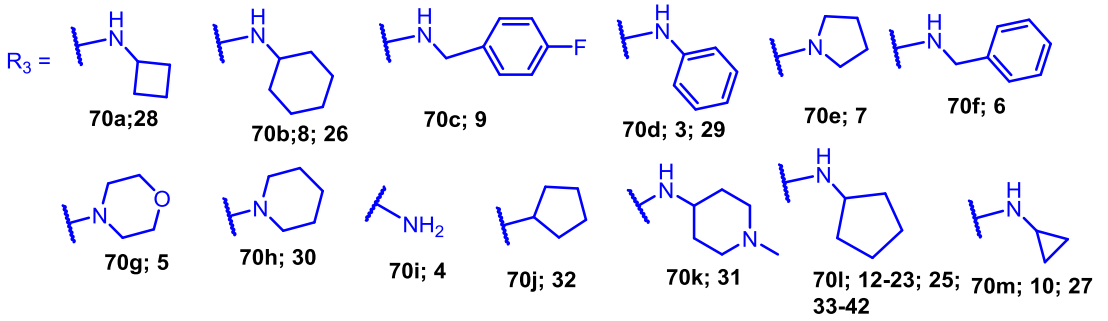

Scheme 1. General synthesis of final compounds 3-42.

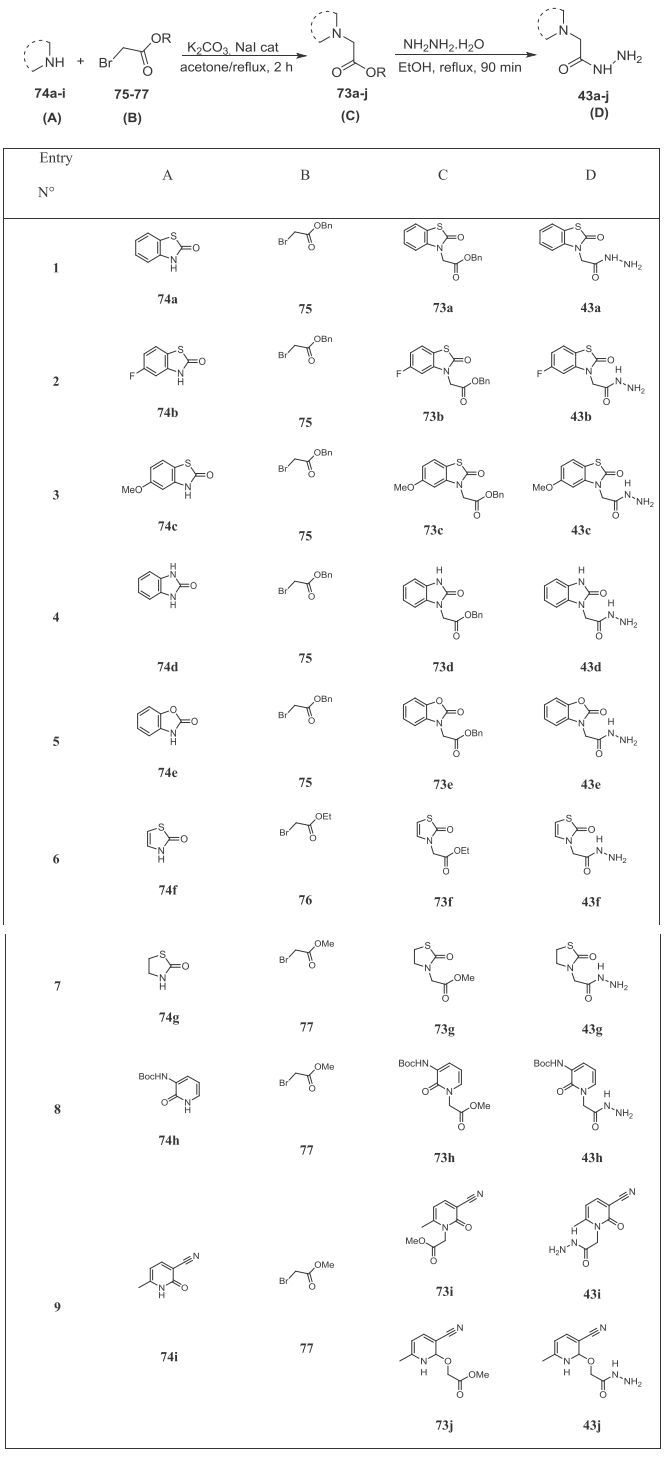

Scheme 2. Synthesis of hydrazides 43a-j.

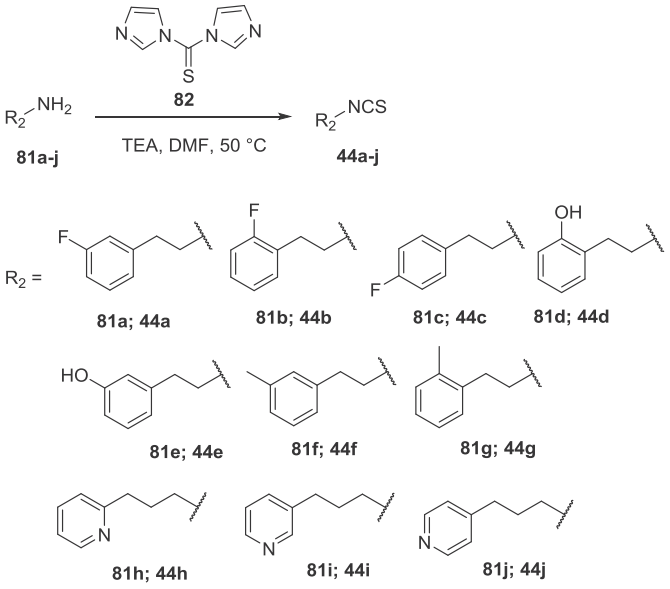

Scheme 3. Synthesis of isothiocyanates 44a-j.

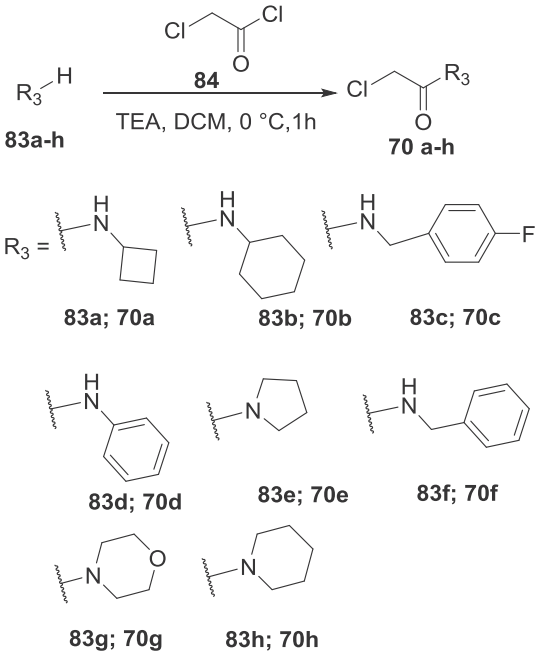

Scheme 4. Synthesis of chloroacetamides 70a-h.

cause appreciable signs of DNA damage.

Overall, these data suggest that disrupting Rad51-BRCA2 interaction could be a valuable strategy for improving olaparib's antitumor profile in cancer cell lines that are usually refractory to the drug. This includes pancreatic cancer, which is a major unmet medical need. Additionally, this study paves the way for the exploitation of the synthetic lethality paradigm in order to discover innovative anticancer therapies based on other lethal gene pairs, using a similar medicinal chemistry strategy.

3. Conclusions

In recent years, innovative anticancer treatments have relied on targeted therapies to improve drug efficacy and reduce side-effects. In parallel, precision medicine has provided a new paradigm for identifying individual patients or groups of patients for treatment with tailored pharmacological medications. For example, PARP inhibitors were recently been approved to treat ovarian cancer in patients with genetic mutations in the BRCA genes (1 and 2). For patients with BRCA2 mutations, the underlying molecular mechanism of action is related to the simultaneous blocking of two DNA repair pathways. Olaparib (the first approved PARPi) chemically inhibits single-strand break repair, while the BRCA2 germline

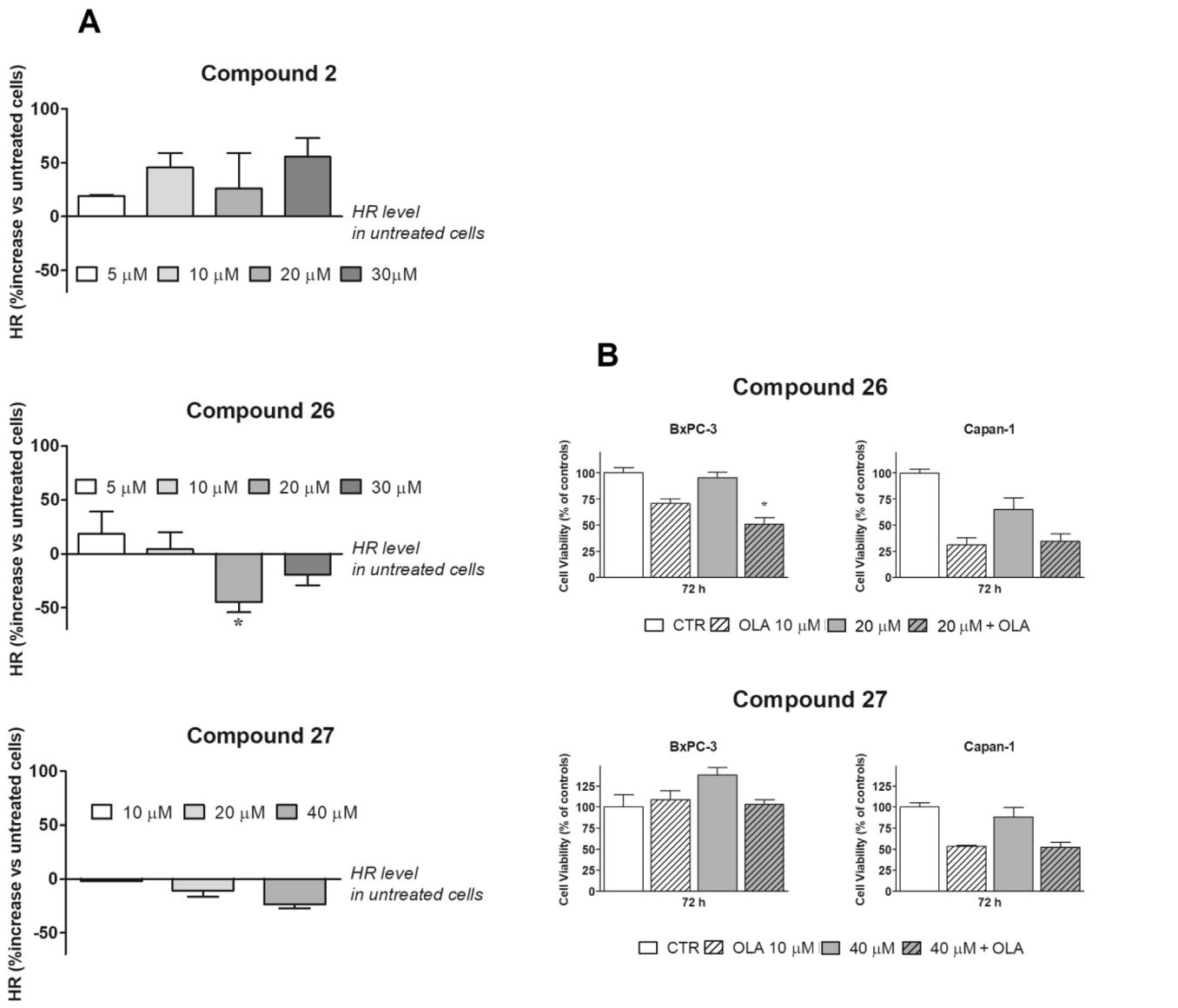

Fig. 4. (A) Estimation of homologous recombination efficiency in BxPC-3 cells treated (16 h) with **2** and with the newly identified BRCA2-Rad51 disruptors **26** and **27**. *, $p < 0.05$ as evaluated by ANOVA followed by Dunnet's post-test. (B) Evaluation of cell viability assessed in combination experiments with olaparib (10 μM) + **26** or **27** on BxPC-3 and Capan-1 cultures. The doses showing the best results in the experiments in Fig. 1A were used. Olaparib concentration was selected on the basis of previous experiments (2). *, $p < 0.05$ as evaluated by ANOVA followed by Dunnet's post-test.

mutations genetically block the double-strand break repair. This has been demonstrated in ovarian cancer (for which olaparib was originally approved), and in clinical trials in breast and pancreatic cancers. Pancreatic cancer is a major unmet medical need. Recently, we reported a new paradigm dubbed "fully small-molecule-induced synthetic lethality." This paradigm was based on the observation that, by using a small organic molecule to disrupt the Rad51-BRCA2 interaction, it is possible to mimic the effect of BRCA2 germline mutations, thus widening the population of patients eligible for treatment with olaparib and other PARPi. In the present study, we further confirmed this concept by investigating the SAR of the previously discovered triazole derivatives. We also improved the biological screening cascade with experiments designed to confirm the molecular mechanism of action (disruption of Rad51-BRCA2 interaction) in cancer cells. We obtained one molecule, **26**, with an improved profile relative to the initial hits (according to a biochemical ELISA essay), and a clear mechanism of action allowing synergy with olaparib in pancreatic cancer cells (BxPC3), where olaparib is normally inactive. In summary, **26** i) inhibited the BRCA2-Rad51 interaction; ii) hit its target and inhibited its function in living cells; iii) significantly increased the therapeutic power of olaparib alone in cells with a functional BRCA2-Rad51 pathway, where usually olaparib is inactive; and iv) increased the formation of double-strand breaks when administered in combination with olaparib.

However, we could not fully reproduce the paradigm of synthetic lethality with **26**. A possible explanation is its low-level potency, which did not cause HR inhibition greater than 40%. In addition, the inherent resistance to apoptosis of BxPC3 cells, which bear a mutant p53 [31], could have further prevented apoptosis. Therefore, further biological experiments and new classes of Rad51-BRCA2 disruptors are needed to confirm this paradigm for

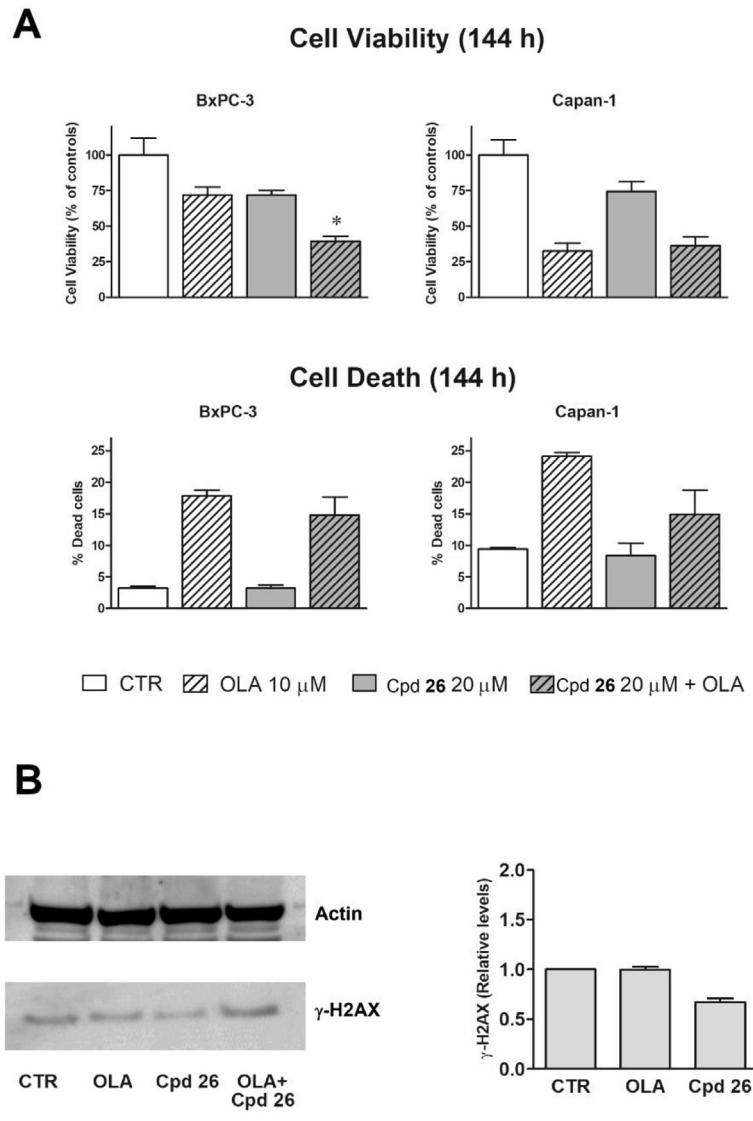

Fig. 5. (A) cell viability and cell death measured in BxPC-3 and Capan-1 cultures after 144 h treatment. **26** significantly increased olaparib's effect on the viability of BxPC-3 cells. *, $p < 0.05$ as evaluated by ANOVA followed by Dunnet's post-test. No effect on cell death was observed. (B) Immunoblotting evaluation of γ-H2AX. The combination olaparib + **26** caused a >70% increased signal of DNA damage (see bar graph).

discovering innovative anticancer therapies.

We are confident that the synthetic lethality framework will provide new pathways, targets, and ideas for identifying small molecules with complex and innovative mechanisms of action as next-generation anticancer therapies.

4. Experimental section

4.1. Chemistry

4.1.1. General chemical methods

Solvents and reagents were obtained from commercial suppliers and used without further purification. If required, solvents were distilled prior to use. For simplicity, solvents and reagents are indicated as follows: acetonitrile (MeCN), 1,8-Diazabicyclo(5.4.0) undec-7-ene (DBU), cyclohexane (Cy), dichloromethane (DCM), diethyl ether (Et_2O), dimethylsulfoxide (DMSO), ethanol (EtOH), ethyl acetate (EtOAc), methanol (MeOH), triethylamine (TEA). Thin-layer chromatography analyses were performed using pre-coated Supelco silica gel on TLC Al foils 0.2 mm and visualized by UV (254 nm), and/or $KMnO_4$ stain. Automated column chromatography purifications were done using a Teledyne ISCO apparatus (CombiFlash® Rf) with pre-packed silica gel columns of different sizes (from 4 g to 120 g). Mixtures of increasing polarity of Cy and EtOAc or DCM and MeOH were used as eluents. Reactions involving microwave irradiation were performed using Explorer® −48 positions instrument (CEM). NMR experiments were run on a Bruker Avance III 400 system (400.13 MHz for ^1H, and 100.62 MHz for ^{13}C), equipped with a BBI probe and Z-gradients. Spectra were acquired at 300 K, using deuterated dimethylsulfoxide (DMSO-d_6) or deuterated chloroform (Chloroform-d) as solvent. Chemical shifts for ^1H and ^{13}C spectra were recorded in parts per million using the residual non-deuterated solvent as the internal standard (for DMSO-d_6: 2.50 ppm, ^1H; 39.52 ppm, ^{13}C; for Chloroform-d: 7.26 ppm, ^1H; 77.16 ppm, ^{13}C). Data are reported as follows: chemical shift (ppm), multiplicity (indicated as: bs, broad signal; s,

singlet; d, doublet; t, triplet; q, quartet; p, quintet; sx, sextet; m, multiplet and combinations thereof), coupling constants (J) in Hertz (Hz) and integrated intensity. UPLC/MS analyses were run on a Waters ACQUITY UPLC/MS system consisting of an SQD (Single Quadrupole Detector) Mass Spectrometer equipped with an Electrospray Ionization interface and a Photodiode Array Detector. PDA range was 210–400 nm. Analyses were performed on an ACQUITY UPLC BEH C18 column (50 × 2.1 mmID, particle size 1.7 μm) with a VanGuard BEH C18 pre-column (5 × 2.1 mmID, particle size 1.7 μm). Mobile phase was 10 mM NH_4OAc in H_2O at pH 5 adjusted with AcOH (A) and 10 mM NH_4OAc in CH_3CN/H_2O (95:5) at pH 5 (B). Electrospray ionization in positive and negative mode was applied. Analyses were performed with a gradient: 5–95% B over 3 min; flow rate 0.5 mL/min; temperature 40 °C. Compounds were named using the naming algorithm developed by CambridgeSoft Corporation and used in ChemBioDraw Ultra 15.0. All final compounds displayed ≥98% purity as determined by UPLC/MS analysis.

PAINS analysis. Compounds **1**–**3**, **16**, **26**–**28**, **34** and **39**, which turned out to be biologically active, were analyzed for known classes of interference compounds. According to the Free ADME-Tox Filtering Tool (FAFDrugs4) program (http://fafdrugs4.mti.univ-paris-diderot.fr/) none of them was recognized to cause pan assay interference.

*4.1.2. General procedure for synthesis of final triazoles (**3**–**42**)*

The appropriate 1,2,4-triazole-3-thiol (**45**–**69**, 1 equiv), 2-chloro-acetamide (**70a-m**, 1.1 equiv), Cs_2CO_3 (1.1 equiv) and NaI (0.05 equiv) were stirred in dry MeCN at 50 °C, and reaction progress was monitored by UPLC/MS. Then water was added, and the final compounds **3**–**42** were purified by washing the precipitated powder or by flash chromatography (Scheme 1).

Below, we report the characterization of the most active compounds. (See also Supplementary data).

N-cyclohexyl-2-((5-((2-oxobenzo[d]thiazol-3(2H)-yl)methyl)-4-(3-phenylpropyl)-4H-1,2,4-triazol-3-yl*)thio)acetamide* ***26.*** 3-((5-mercapto-4-(3-phenylpropyl)-4H-1,2,4-triazol-3-yl)methyl)benzo[*d*]thiazol-2(3H)-one **59** (80 mg, 0.21 mmol), 2-chloro-N-cyclohexylacetamide **70b** (40 mg, 0.23 mmol), Cs_2CO_3 (75 mg, 0.23 mmol), and a catalytic amount of NaI in 8 mL of dry MeCN were allowed to react for 4 h according to general procedure. The desired product precipitated from water, and 3-((5-mercapto-4-(3-phenylpropyl)-4H-1,2,4-triazol-3-yl)methyl)benzo[*d*]thiazol-2(3H)-one washed with water, Et_2O and dried. Precipitate was purified by column chromatography, solvent system: cyclohexane/EtOAC. Clean compound eluted with EtOAc 100%, to give **26** (89 mg, 80% yield) as a white solid. ^{1}H NMR (400 MHz, DMSO-d_6) δ 7.99 (d, J = 7.7 Hz, 1H), 7.69 (dd, J = 7.8, 1.2 Hz, 1H), 7.47 (dd, J = 8.2, 1.1 Hz, 1H), 7.36 (td, J = 7.8, 1.3 Hz, 1H), 7.30–7.17 (m, 6H), 5.39 (s, 2H), 4.06 (t, 2H), 3.82 (s, 2H), 3.47–3.49 (m, 1H), 2.59 (t, 2H), 1.87–1.79 (m, 2H), 1.63–1.58 (m, 4H), 1.23–1.02 (m, 6H) ppm. ^{13}C NMR (101 MHz, DMSO-d_6) δ 169.1, 165.53, 150.3, 150.2, 140.5, 136.5, 128.3 (2C), 128.1 (2C), 126.6, 126.0, 123.6, 122.9, 121.2, 112.1, 47.9, 43.6, 37.0, 36.9, 32.1 (2C), 32.0, 31.0, 25.1, 24.3 (2C) ppm. UPLC-MS (ESI, m/z) Rt = 2.45 min–522 $(M + H)^+$; UPLC-MS purity (UV 215 nm): >99.5%

N-cyclopropyl-2-((5-((2-oxobenzo[d]thiazol-3(2H)-yl)methyl)-4-(3-phenylpropyl)-4H-1,2,4-triazol-3-yl*)thio)acetamide* ***27.*** 3-((5-mercapto-4-(3-phenylpropyl)-4H-1,2,4-triazol-3-yl)methyl)benzo[*d*]thiazol-2(3H)-one **59** (100 mg, 0.26 mmol), 2-chloro-N-cyclopropylacetamide **70m** (39 mg, 0.29 mmol), Cs_2CO_3 (95 mg, 0.29 mmol) and a catalytic amount of NaI in 5 mL of dry MeCN were allowed to react overnight according to general procedure. The desired product precipitated from water, and was washed with water, Et_2O and dried overnight under vacuum at 60 °C to give **27** (120 mg, quantitative yield) as a white powder. ^{1}H NMR (400 MHz, DMSO-d_6) δ 8.23 (d, J = 4.1 Hz, 1H), 7.70 (dd, J = 7.8, 1.2 Hz, 1H), 7.48–7.46 (m, 2H), 7.36 (td, J = 7.8, 1.3 Hz, 1H), 7.30–7.17 (m, 7H), 5.39 (s, 2H), 4.05 (t, J = 7.9 Hz, 2H), 3.81 (s, 2H), 2.61–2.53 (m, 3H), 1.87–1.79 (m, 2H), 0.59–0.54 (m, 2H), 0.34–0.30 (m, 2H) ppm. ^{13}C NMR (101 MHz, DMSO-d_6) δ 169.1, 167.6, 150.3, 150.2, 140.5, 136.5, 128.4 (2C), 128.1 (2C), 126.6, 126.0, 123.6, 122.9, 121.2, 112.1, 43.6, 36.9, 36.5, 32.0, 31.0, 22.5, 5.5 (2C) ppm. UPLC-MS (ESI, m/z) Rt = 2.15 min–480 $(M + H)^+$; UPLC-MS purity (UV 215 nm): >99.5%.

N-cyclobutyl-2-((5-((2-oxobenzo[d]thiazol-3(2H)-yl)methyl)-4-(3-phenylpropyl)-4H-1,2,4-triazol-3-yl*)thio)acetamide* ***28.*** 3-((5-mercapto-4-(3-phenylpropyl)-4H-1,2,4-triazol-3-yl)methyl)benzo[*d*]thiazol-2(3H)-one **59** (100 mg, 0.26 mmol), 2-chloro-N-cyclobutylacetamide **70a** (43 mg, 0.29 mmol), Cs_2CO_3 (95 mg, 0.29 mmol) and a catalytic amount of NaI in 5 mL of dry MeCN were allowed to react overnight according to general procedure. The desired product precipitated from water, and was washed with water, Et_2O and dried. Precipitate was purified by column chromatography, solvent system: DCM/MeOH. Clean compound eluted with MeOH 4%, to give **28** (102 mg, 79% yield) as a white solid. ^{1}H NMR (400 MHz, DMSO-d_6) δ 8.39 (d, J = 7.6 Hz, 1H), 7.69 (dd, J = 7.8, 1.2 Hz, 1H), 7.47 (dd, J = 8.1, 1.1 Hz, 1H), 7.41–7.29 (m, 1H), 7.32–7.16 (m, 6H), 5.39 (s, 2H), 4.14–4.07 (m, 1H), 4.06–4.03 (m, 2H), 3.82 (s, 2H), 2.62–2.55 (m, 2H), 2.13–1.98 (m, 2H), 1.90–1.69 (m, 4H), 1.64–1.50 (m, 2H) ppm. ^{13}C NMR (101 MHz, DMSO) δ 169.1, 165.3, 150.3, 140.5136.6, 128.4 (2C), 128.1 (2C), 126.6, 126.0, 123.6, 122.9, 121.2, 112.1, 99.5, 43.6, 43.5, 36.9, 36.7, 32.0, 31.0, 30.0 (2C), 14.6 ppm. UPLC-MS (ESI, m/z) Rt = 2.25 min–494 $(M + H)^+$; UPLC-MS purity (UV 215 nm): >99.5%.

2-((5-(((3-cyano-6-methylpyridin-2-yl*)oxy)methyl)-4-(3-phenylpropyl)-4H-1,2,4-triazol*-3-yl*)thio)-N-cyclopentylacetamide* ***39.*** 2-((5-mercapto-4-(3-phenylpropyl)-4H-1,2,4-triazol-3-yl)methoxy)-6-methylnicotinonitrile **66** (140 mg, 0.38 mmol), 2-chloro-N-cyclopentylacetamide **70l** (68 mg, 0.42 mmol), Cs_2CO_3 (137 mg, 0.42 mmol) and a catalytic amount of NaI in 5 mL of dry MeCN were allowed to react for 4 h according to general procedure. The desired product precipitated from water, then it was washed with water, Et_2O and dried. Precipitate was purified by flash chromatography, solvent system: DCM/EtOAc. Clean compound eluted with EtOAc 100%, to give **39** (134 mg, 71% yield) as a white solid. ^{1}H NMR (400 MHz, DMSO-d_6) δ 8.19 (d, J = 7.8 Hz, 1H), 8.16 (br, 1H), 7.23–7.16 (m, 4H), 7.16–7.09 (m, 2H), 5.54 (s, 2H), 4.04 (t, 2H), 4.00–3.92 (m, 1H), 3.90 (s, 2H), 2.64 (t, J = 7.6 Hz, 2H), 2.10–1.99 (m, 2H), 1.81–1.67 (m, 2H), 1.65–1.53 (m, 2H), 1.53–1.41 (m, 2H), 1.41–1.27 (m, 2H) ppm. ^{13}C NMR (101 MHz, DMSO) δ 165.9, 161.9, 161.3, 150.6, 144.1, 140.4, 128.2 (2C), 128.1 (2C), 128.0, 125.9, 117.4, 115.2, 92.4, 57.9, 50.7, 43.5, 36.7, 32.1 (2C), 32.0, 30.8, 24.3, 23.3 (2C) ppm. UPLC-MS (ESI, m/z) Rt = 2.24 min–491 $(M + H)^+$; UPLC-MS purity (UV 215 nm): >99.5%.

*4.1.3. Synthetic procedures to obtain hydrazides **43a-j***

*4.1.3.1. General procedure for synthesis of esters **(73a-j)**.* A mixture of appropriate amine **74a-i** (1 equiv), K_2CO_3 (1.05 equiv), and a catalytic amount of NaI in acetone was stirred at room temperature. Benzyl, ethyl, or methyl bromoacetate **75**, **76**, **77** (1.1 equiv) was added dropwise to the mixture, which was then refluxed for 2 h (Scheme 2, see also Supplementary data).

The ester **73a** was synthesized as previously described [24].

Benzyl 2-(5-fluoro-2-oxobenzo[d]thiazol-3(2H)-yl)acetate ***(73b).*** 5-fluorobenzo[*d*]thiazol-2(3H)-one **74b** (800 mg, 4.73 mmol), K_2CO_3 (687 mg, 4.96 mmol), benzyl bromoacetate **75** (810 μL, 5.21 mmol), and a catalytic amount of NaI in acetone (8 mL) were allowed to react according to the general procedure.

The reaction was cooled down, water added, and aqueous phases extracted with EtOAc (3 × 10 mL). The collected organic phases were washed with brine, dried over $MgSO_4$, filtered, and

evaporated in vacuo to give crude **73b** (1.78 g) which was used in the next step without further purification. ^{1}H NMR (400 MHz, DMSO-d_6) δ 7.78–7.71 (m, 1H), 7.46–7.40 (m, 1H), 7.40–7.35 (m, 5H), 7.15–7.07 (m, 1H), 5.21 (s, 2H), 4.94 (s, 2H) ppm. UPLC-MS (ESI, *m/z*) Rt = 2.37 min–318 $(M + H)^+$.

*4.1.3.2. General procedure for synthesis of hydrazides **(43a-j)**.* The appropriate ester **73a-j** (1.0 equiv) was dissolved in 15 mL of EtOH and hydrazine hydrate (23 equiv) was added. The reaction was left to stir at room temperature for 5–12 h. The reaction was stopped, solvent evaporated under vacuum to obtain crude hydrazide, which was used in the next step without further purification.

The hydrazide **43a** was synthesized as previously described [24].

*2-(5-fluoro-2-oxobenzo[d]thiazol-3(2H)-yl)acetohydrazide **(43b).*** **73b** (115 mg, 0. 63, 1 equiv) was suspended in EtOH and hydrazine hydrate (150 μL, 3.15 mmol, 4 equiv) was added. The mixture was left to stir at room temperature for 5 h. Then reaction was stopped, and solvent evaporated under vacuum to obtain crude **43b** (150 mg), which was used in the next step without further purification. UPLC-MS (ESI, *m/z*) Rt = 1.28 min–242 $(M + H)^+$.

*4.1.4. General procedure for synthesis of isothiocyanates **(44a-j)***

1, 1-thiocarbonyldiimidazole **82** (1.2 equiv) was dissolved in dry DMF at 50 °C. To this mixture, a solution of the appropriate amines **81a-j** (1 equiv) and dry Et_3N (1 equiv) in dry DMF was slowly added dropwise. The mixture was stirred at 50 °C, and the progress monitored by TLC or UPLC/MS. Then the reaction was cooled down, water was added, and the aqueous phase was extracted with EtOAc (3 × 10 mL). Organic phases were washed with water and brine, dried over Na_2SO_4, filtered, and concentrated in vacuo. Purification by flash column chromatography was performed.

*1-fluoro-3-(2-isothiocyanatoethyl)benzene **(44a).*** 1, 1-thiocarbonyldiimidazole **82** (769 mg, 4.32 mmol), 2-(3-fluorophenyl)ethan-1-amine **81a** (470 μL, 3.60 mmol), and Et_3N (500 μL, 3.60 mmol) in DMF (6 mL+1 mL) were allowed to react according to the general procedure for 1 h. Crude was purified by flash chromatography, solvent system cyclohexane/EtOAc. Clean compound was eluted with EtOAc 30% yielding **44a** (342 mg, 52% yield) as a pale yellow oil. ^{1}H NMR (400 MHz, DMSO-d_6) δ 7.44–7.34 (m, 1H), 7.21–7.06 (m, 3H), 3.94 (t, *J* = 6.6 Hz, 2H), 3.00 (t, *J* = 6.6 Hz, 2H) ppm.

*4.1.5. General procedures for the synthesis of triazoles **45–69***

A mixture of hydrazide **43a-n** (1.0 equiv) and the appropriate isothiocyanate **44a-l** (1.1 equiv) in EtOH containing TEA (2.1 equiv) was refluxed overnight. When the UPLC/MS analysis revealed about 1/1 open/cyclized product, the reaction mixtures were evaporated, suspended in dioxane (20 mL), 0.5 mL of DBU added, and heated at 150 °C for 20 min under microwave.

Triazole **45** and **59** were prepared as described in a previous paper [24].

*2-((5-mercapto-4-(3-phenylpropyl)-4H-1,2,4-triazol-*3-yl*) methoxy)-6-methylnicotinonitrile **(66).*** A mixture of hydrazide **43j** (200 mg, 0.97 mmol) and commercially available (3-isothiocyanatopropyl)benzene **44l** (177 μL, 1.07 mmol) in 10 mL of ethanol containing TEA (285 μL, 2.04 mmol) were allowed to react according to general procedure. After refluxing overnight, the reaction was cooled and solvent evaporated. The crude was purified by flash chromatography (cyclohexane/EtOAc from 100:0 to 60:40) to give **66** (145 mg, 41% yield) as a white solid. ^{1}H NMR (400 MHz, DMSO-d_6) δ 13.88 (s, 1H), 8.20 (d, *J* = 7.7 Hz, 1H), 7.24–6.96 (m, 7H), 5.46 (s, 2H), 4.09–3.90 (m, 2H), 2.63 (t, *J* = 7.6 Hz, 2H), 2.48 (s, 3H), 2.17–2.03 (m, 2H) ppm. UPLC-MS (ESI, *m/z*) Rt = 2.19 min–366 $(M + H)^+$.

*4.1.6. General procedure for synthesis of chloroacetamides (**70a-h**)*

To the appropriate substituted amines (**83a-h,** 1 equiv) in DCM was added chloroacetyl chloride **84** (1.1 equiv) followed by the addition of TEA (2.8 equiv) at 0–10 °C. The reaction was continued at the same temperature for 1 h. Then, the reaction mixture was washed with saturated $NaHCO_3$ solution, HCl 2N, and brine solution. The excess of organic solvent was removed under reduced pressure and the crude compounds were purified by flash chromatography, eluting with Cyclohexane/EtOAc 1/1.

2-chloro-N-cyclobutylacetamide **(70a).** Cyclobutylamine **83a** (240 μL, 2.81 mmol), chloroacetyl chloride **84** (248 μL, 3.12 mmol), TEA (1.09 mL, 7.8 mmol) in DCM (6 mL) were allowed to react according to the general procedure. Clean compound was eluted with Cycloexane/EtOAc 7/3, giving **70a** (380 mg, 83% yield) as white solid. ^{1}H NMR (400 MHz, DMSO-d_6) δ 8.43 (s, 1H), 4.28–4.09 (m, 1H), 3.98 (s, 2H), 2.21–2.08 (m, 2H), 2.00–1.80 (m, 2H), 1.70–1.59 (m, 2H) ppm. UPLC-MS (ESI, *m/z*) Rt = 1.23 min–148 [M (^{35}Cl) +H]$^+$.

*2-chloro-N-cyclohexylacetamide **(70b).*** Cyclohexylamine **83b** (911 μL, 7.97 mmol), chloroacetyl chloride **84** (705 μL, 8.85 mmol), TEA (3.08 mL, 22.14 mmol) in DCM (20 mL) were allowed to react, and clean compound was purified according to the general procedure, giving **70b** (995 mg, 71% yield) as white solid. ^{1}H NMR (400 MHz, Chloroform-d) δ 6.45 (s, 1H), 4.04 (s, 2H), 3.89–3.72 (m, 1H), 1.94 (dq, *J* = 12.0, 3.7 Hz, 2H), 1.74 (dp, *J* = 10.5, 3.5, 2.9 Hz, 2H), 1.64 (dq, *J* = 12.7, 3.5 Hz, 1H), 1.48–1.31 (m, 2H), 1.21 (dddt, *J* = 15.4, 11.4, 7.2, 3.4 Hz, 3H) ppm. UPLC-MS (ESI, *m/z*) Rt = 1.82 min–178 [M (^{37}Cl) +H]$^+$, 176 [M (^{35}Cl) +H]$^+$.

4.2. Biology

4.2.1. ELISA assay

A competitive ELISA screening assay using biotinylated BRC4 peptide to disrupt the BRC4–RAD51 interaction was performed by modifying the method described by Rajendra et al. [32].

BRC4-biotinylated peptide (N-term BiotinKEPTLLGFHTASGKKVKIAKESLDKVKNLFDEKEQ from Life Technologies) was used to coat 384-well plates (Nunc). After washing with PBS containing 0.05% Tween-20 (PBST), and blocking with the solution BSA 1%/PBST, overnight hybridization with human Rad51 protein (NP_002866 Creative Biomart, NY) was performed. Test compounds were added in dose-response from 0.01 to 100 μM in triplicate with constant DMSO 1%. Antibody raised against Rad51 (Millipore) and HRP-secondary antibody staining to develop the 3,3′,5,5′-tetramethyllbenzidine signal (Sigma) quenched with 1M HCl was used as the assay readout. Colorimetric measure was read on Victor5 (PerkinElmer) plate Reader. BRC4 and Rad51 were included in the assay as positive control. Results were analyzed using GraphPad Software.

4.2.2. Cell culture and treatments

BxPC-3 and Capan-1 cells were grown in RPMI 1640 containing 10% FBS, 100 U/ml penicillin/streptomycin, 2 mM glutamine. All media and supplements were from Sigma-Aldrich. Cultures were routinely tested for Mycoplasma contamination. Treatments (olaparib and BRCA2-Rad51 disruptors) were administered in culture medium supplemented with 0.6% DMSO. The same amount of DMSO was added to the control, untreated cultures.

4.2.3. Homologous recombination assay

Homologous recombination (HR) was assessed by using a commercially available assay (Norgen). This assay is based on cell transfection with two plasmids that, upon cell entry, integrate in genomic DNA and recombinate. The efficiency of HR can be assessed by PCR, using primer mixtures included in the assay kit.

Different primer mixtures allow differentiation between the original plasmid backbones and their recombination product.

BxPC3 cells (3×10^5 per well) were seeded in a 24-well plate and allowed to adhere overnight. Co-transfection with the two plasmids was performed in Lipofectamine 2000 (Invitrogen), according to the manufacturer's instructions. After 5 h, transfection medium was removed, and cells were exposed for 16 h at different doses of inhibitors, dissolved in RPMI in the presence of 0.6% DMSO. After washing with PBS, cells were harvested, and DNA was isolated using Illustra™ Tissue and Cell Genomic Prep Mini Spin kit (GE Healthcare). Sample concentration was measured using an ONDA Nano Genius photometer.

PCR was performed according to the manufacturer's instructions, using 100–150 ng of template. The amplicons of plasmid backbones and of recombination product were separated by electrophoresis on 2% agarose gel. Band intensity was measured by a Kodak Electrophoresis Documentation and Analysis System and used to evaluate HR efficiency, which is given by the ratio: [Recombination Product/Backbone Plasmids].

4.2.4. Cell viability assay

Cell viability was assessed by Crystal Violet staining. BxPC-3 and Capan-1 cells (5×10^3-10^4/well) were plated in 96-well plates and treated (72–144 h) with olaparib (10 μM), given alone or in combination with **26** (20 μM). At the end of treatment, cell culture medium was removed, the cells were washed with PBS, fixed in Glutaraldehyde 1% in PBS for 15 min at room temperature, and rinsed with PBS several times. Then, the samples were incubated in 0.01% Crystal Violet for 30 min and washed in PBS. To each well was added 100 μL cold ethanol 70% and the absorbance measured in a microplate reader (Bio-Rad, Hercules, CA, USA) at 570 nm. The results were expressed as a percentage of viable cells on control.

4.2.5. Cytotoxicity assay

Cell death was assessed by applying the CellTox™ Green Cytotoxicity assay (Promega). Briefly, BxPC-3 and Capan-1 cells (5×10^3/well) were plated in 96-well plates and treated for 144 h with olaparib (10 μM), given alone or in combination with **26** (20 μM). At the end of treatment, the CellTox™ dye was added to cell cultures and the green fluorescence signal, which is produced by the binding interaction with dead cell DNA, was measured following the manufacturer's instructions.

4.2.6. Western blot

Cell cultures (1.5×10^6 cells) were exposed for 144 h to olaparib (10 μM), given alone or in combination with **26** (20 μM). Cells were then lysed in 100 μL RIPA buffer containing protease and phosphatase inhibitors (Sigma Aldrich). The homogenates were left 30 min on ice and then centrifuged 15 min at 10000 g. 50 μg proteins of the supernatants (measured according to Bradford) were loaded into 12% polyacrylamide gel for electrophoresis. The separated proteins were blotted on a low fluorescent PVDF membrane (GE Lifescience) using a standard apparatus for wet transfer with an electrical field of 80 mA for 16 h. The blotted membrane was blocked with 5% BSA in TBS-Tween and probed with the primary antibody. The antibodies used were: rabbit anti-γH2AX [phospho S139] (Abcam), rabbit anti-Actin (Sigma Aldrich). Binding was revealed by a Cy5-labelled secondary antibody (anti rabbit-IgG, GE Lifescience; anti mouse-IgG, Jackson Immuno-Research). All incubation steps were performed according to the manufacturer's instructions. Fluorescence of the blots was assayed with the Pharos FX scanner (BioRad) at a resolution of 100 μm, using the Quantity One software (BioRad).

Acknowledgments

We thank the Italian Institute of Technology and the University of Bologna for financial support. We thank Prof. Maurizio Recanatini for fruitful discussions.

Appendix A. Supplementary data

Supplementary data to this article can be found online at https://doi.org/10.1016/j.ejmech.2019.01.008.

References

[1] M.N. Patel, M.D. Halling-Brown, J.E. Tym, P. Workman, B. Al-Lazikani, Objective assessment of cancer genes for drug discovery, Nat. Rev. Drug Discov. 12 (2013) 35–50.
[2] B. Vogelstein, N. Papadopoulos, V.E. Velculescu, S. Zhou, L.A. Diaz Jr., et al., Cancer genome landscapes, Science 339 (2013) 1546–1558.
[3] B.J. Druker, M. Talpaz, D.J. Resta, B. Peng, E. Buchdunger, et al., Efficacy and safety of a specific inhibitor of the BCR-ABL tyrosine kinase in chronic myeloid leukemia, N. Engl. J. Med. 344 (2001) 1031–1037.
[4] B.J. Druker, F. Guilhot, S.G. O'Brien, I. Gathmann, H. Kantarjian, et al., Five-year follow-up of patients receiving imatinib for chronic myeloid leukemia, N. Engl. J. Med. 355 (2006) 2408–2417.
[5] M.J. Moore, D. Goldstein, J. Hamm, A. Figer, J.R. Hecht, et al., Erlotinib plus gemcitabine compared with gemcitabine alone in patients with advanced pancreatic cancer: a phase III trial of the National Cancer Institute of Canada Clinical Trials Group, J. Clin. Oncol. 25 (2007) 1960–1966.
[6] B. Escudier, A. Pluzanska, P. Koralewski, A. Ravaud, S. Bracarda, et al., Bevacizumab plus interferon alfa-2a for treatment of metastatic renal cell carcinoma: a randomised, double-blind phase III trial, Lancet 370 (2007) 2103–2111.
[7] R.J. Motzer, M.D. Michaelson, B.G. Redman, G.R. Hudes, G. Wilding, et al., Activity of SU11248, a multitargeted inhibitor of vascular endothelial growth factor receptor and platelet-derived growth factor receptor, in patients with metastatic renal cell carcinoma, J. Clin. Oncol. 24 (2006) 16–24.
[8] J.M. Llovet, S. Ricci, V. Mazzaferro, P. Hilgard, E. Gane, et al., Sorafenib in advanced hepatocellular carcinoma, N. Engl. J. Med. 359 (2008) 378–390.
[9] P.A. Janne, N. Gray, J. Settleman, Factors underlying sensitivity of cancers to small-molecule kinase inhibitors, Nat. Rev. Drug Discov. 8 (2009) 709–723.
[10] T. Force, K.L. Kolaja, Cardiotoxicity of kinase inhibitors: the prediction and translation of preclinical models to clinical outcomes, Nat. Rev. Drug Discov. 10 (2011) 111–126.
[11] A. Gupta, A. Ahmad, A.I. Dar, R. Khan, Synthetic lethality: from research to precision cancer nanomedicine, Curr. Cancer Drug Targets 18 (2017) 337–346.
[12] W.G. Kaelin Jr., The concept of synthetic lethality in the context of anticancer therapy, Nat. Rev. Canc. 5 (2005) 689–698.
[13] D.A. Chan, A.J. Giaccia, Harnessing synthetic lethal interactions in anticancer drug discovery, Nat. Rev. Drug Discov. 10 (2017) 351–364.
[14] R. Beijersbergen, L. Wessel, R. Bernards, Synthetic lethality in cancer therapeutics, Annu. Rev. Cell Biol. 1 (2017) 141–161.
[15] E.D. Deeks, Olaparib: first global approval, Drugs 75 (2015) 231–240.
[16] B. Kaufman, R. Shapira-Frommer, R.K. Schmutzler, M.W. Audeh, M. Friedlander, et al., Olaparib monotherapy in patients with advanced cancer and a germline BRCA1/2 mutation, J. Clin. Oncol. 33 (2015) 244–250.
[17] A.A. Davies, J.Y. Masson, M.J. McIlwraith, A.Z. Stasiak, A. Stasiak, et al., Role of BRCA2 in control of the RAD51 recombination and DNA repair protein, Mol. Cell 7 (2001) 273–282.
[18] H.L. Klein, The consequences of Rad51 overexpression for normal and tumor cells, DNA Repair 7 (2008) 686–693.
[19] R. Roy, J. Chun, S.N. Powell, BRCA1 and BRCA2: different roles in a common pathway of genome protection, Nat. Rev. Canc. 12 (2012) 68–78.
[20] J. Nomme, A. Renodon-Corniere, Y. Asanomi, K. Sakaguchi, A.Z. Stasiak, et al., Design of potent inhibitors of human RAD51 recombinase based on BRC motifs of BRCA2 protein: modeling and experimental validation of a chimera peptide, J. Med. Chem. 53 (2010) 5782–5791.
[21] L. Pellegrini, D.S. Yu, T. Lo, S. Anand, M. Lee, et al., Insights into DNA recombination from the structure of a RAD51-BRCA2 complex, Nature 420 (2002) 287–293.
[22] J. Zhu, L. Zhou, G. Wu, H. Konig, X. Lin, et al., A novel small molecule RAD51 inactivator overcomes imatinib-resistance in chronic myeloid leukaemia, EMBO Mol. Med. 5 (2013) 353–365.
[23] W.H. Lee, P.L. Chen, J. Zhu, Composition and methods for disruption of BRCA-RAD51 interaction, 2006. WO 2006/044933 A2, April 27.
[24] F. Falchi, E. Giacomini, T. Masini, N. Boutard, L. Di Ianni, et al., Synthetic lethality triggered by combining olaparib with BRCA2-Rad51 disruptors, ACS Chem. Biol. 12 (2017) 2491–2497.
[25] D.E. Scott, A.R. Bayly, C. Abell, J. Skidmore, Small molecules, big targets: drug discovery faces the protein-protein interaction challenge, Nat. Rev. Drug Discov. 15 (2016) 533–550.

[26] H.C. Bertrand, M. Schaap, L. Baird, N.D. Georgakopoulos, A. Fowkes, et al., Design, synthesis, and evaluation of triazole derivatives that induce Nrf2 dependent gene products and inhibit the Keap1-nrf2 protein-protein interaction, J. Med. Chem. 58 (2015) 7186–7194.
[27] T.R. Reddy, C. Li, P.M. Fischer, L.V. Dekker, Three-dimensional pharmacophore design and biochemical screening identifies substituted 1,2,4-triazoles as inhibitors of the annexin A2-S100A10 protein interaction, ChemMedChem 7 (2012) 1435–1446.
[28] L. Yan, J. Liang, C. Yao, P. Wu, X. Zeng, et al., Pyrimidine triazole thioether derivatives as toll-like receptor 5 (TLR5)/Flagellin complex inhibitors, ChemMedChem 11 (2016) 822–826.
[29] D.W. Abbott, M.L. Freeman, J.T. Holt, Double-strand break repair deficiency and radiation sensitivity in BRCA2 mutant cancer cells, J. Natl. Cancer Inst. 90 (1998) 978–985.
[30] J.S. Dickey, C.E. Redon, A.J. Nakamura, B.J. Baird, O.A. Sedelnikova, et al., H2AX: functional roles and potential applications, Chromosoma 118 (2009) 683–692.
[31] E.L. Deer, J. Gonzalez-Hernandez, J.D. Coursen, J.E. Shea, J. Ngatia, et al., Phenotype and genotype of pancreatic cancer cell lines, Pancreas 39 (2010) 425–435.
[32] E. Rajendra, A.R. Venkitaraman, Two modules in the BRC repeats of BRCA2 mediate structural and functional interactions with the RAD51 recombinase, Nucleic Acids Res. 38 (2010) 82–96.